Article published online: 2025-02-13

Review Article

Multimodality Imaging in Wrist Fractures and Dislocations

Madhurima Sharma[1] Shayeri Roy Choudhury[1] Anindita Sinha[1] Mahesh Prakash[1]

[1] Departments of Radiodiagnosis and Imaging, Post Graduate Institute of Medical Education and Research, Chandigarh, India

Indian J Radiol Imaging

Address for correspondence Anindita Sinha, MD, Department of Radiodiagnosis, Post Graduate Institute of Medical Education and Research, Chandigarh 160012, India (e-mail: dranindita@gmail.com).

Abstract

Wrist fractures and dislocations are frequently encountered in the emergency department and can cause significant long-term disability. Imaging plays a crucial role in the evaluation of wrist injuries, with conventional radiography being the first imaging investigation. Cross-sectional imaging is playing an increasingly important role in management of wrist injuries. Computed tomography with 3D and multiplanar reformatting capabilities is in particular useful for detailed evaluation of bony injuries and can provide vital information to orthopaedic surgeons for adequate surgical planning. In this article, we provide a brief review of the normal wrist anatomy, imaging appearance, and various patterns of fractures and dislocations commonly encountered in the emergency department.

Keywords

- wrist injuries
- wrist trauma
- radius fractures
- radiography
- computed tomography

Introduction

The wrist is a complex joint with multiple articulations among the radius, ulna, carpal bones, and base of the metacarpals, reinforced by important ligamentous support structures and soft tissues. Fractures of the wrist account for a significant number of admissions in the emergency department on a regular basis. In the absence of timely diagnosis and treatment, traumatic wrist injuries can result in significant functional impairment and long-term debilitating sequelae such as nonunion, degenerative arthritis, and avascular necrosis. Conventional radiography is the primary radiological investigation in acute wrist trauma; however, due to the overlap of multiple bones and intricate anatomy of the differently shaped bones, radiographs may not always be adequate in diagnosing injuries. Computed tomography (CT) is the modality of choice for evaluation of suspected bony injuries of the wrist in case of negative or indeterminate radiographs. Also, multiplanar and volumetric reformations are useful in detailed fracture evaluation and preoperative planning. CT is easily available in the emergency department and provides quick and accurate results in trauma patients. Magnetic resonance imaging (MRI) has limited role in acute fractures and dislocations. However, it is particularly useful in the evaluation of soft tissue injuries.

Structural complexity of the wrist joint warrants an understanding of the detailed anatomy of the osseous and soft tissue structures, their appearance on various imaging modalities, and identification of abnormalities that point toward important traumatic pathologies. In this article, we discuss normal anatomy and imaging appearance of the wrist with illustration of various traumatic fractures and dislocations.

Anatomy of Wrist Joint

The wrist joint is comprised of the distal end of the radius and the proximal carpus (forming the radiocarpal joint), the distal end of the ulna, and the triangular fibrocartilaginous ligament forming a complex condyloid joint (►**Fig. 1**). This

DOI https://doi.org/10.1055/s-0044-1801268.
ISSN 0971-3026.

Thieme Medical and Scientific Publishers Pvt. Ltd., A-12, 2nd Floor, Sector 2, Noida-201301 UP, India

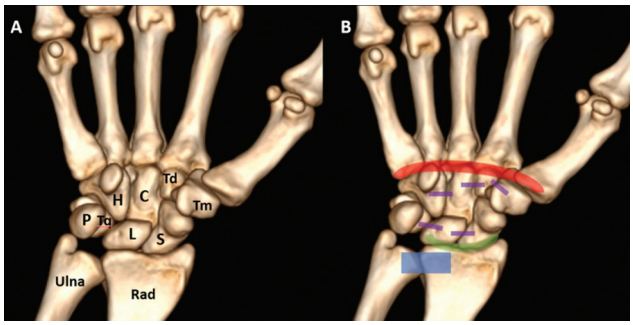

Fig. 1 (A) Volume rendered computed tomography (CT) image showing the normal bony anatomy of the wrist. C, capitate; H, hamate; L, lunate; P, pisiform; Rad, radius; S, scaphoid; Td, trapezoid; Tm, trapezium; Tq, triquetral. (**B**) Volume-rendered CT image showing various joints of the wrist: distal radioulnar joint (*blue*), radiocarpal joint (*green*), intercarpal joints (*purple*), and carpometacarpal joints (*red*).

allows for movement in two axes, namely, flexion–extension and adduction–abduction.

Distal Radioulnar Joint

The distal radioulnar joint (DRUJ) is a synovial type of pivot joint formed between the lateral surface of the ulnar head and the sigmoid notch.[1] The concave sigmoid notch allows radial movement around the ulnar head in pronation and supination. The osseous component only contributes to 20% of the joint stability. The soft tissues, specifically the triangular fibrocartilaginous complex (TFCC), contributes largely to the dynamic stabilization at the DRUJ.[2]

Carpal Bones

Eight carpal bones in two rows articulate to form the carpus.[3] The proximal row constitutes from the radial to the ulnar side the scaphoid, lunate, triquetral, and pisiform (which does not articulate with any other bone and is seen in a separate plane volar to the triquetral). The distal arc includes the trapezium, trapezoid, capitate, and hamate bones (►**Fig. 1**). Together with the extrinsic and intrinsic ligaments, they form a static and dynamic stabilizer of the wrist joint, allowing for a wide range of movements.

Carpal arcs (or Gilula arcs) are three arcs on a posteroanterior (PA) radiograph determining the proper alignment of the carpus. The first arc is seen outlining the proximal margin of the proximal carpus (scaphoid, lunate, and trapezium). The second arc outlines the distal margin of the proximal carpus, and the third arc outlines the proximal margin of the capitate and the hamate (►**Fig. 2**). Loss of congruency of any of these arcs suggests an abnormality at that site.

Ligaments around the Wrist Joint

A detailed discussion of ligamentous anatomy is beyond the scope of this article. The ligaments of the wrist joint are divided into intrinsic and extrinsic ligaments.[4] The intrinsic ligaments solely attached to the carpal bones, while the extrinsic ligaments extend between the forearm bones, tendon sheaths, etc. The three main intrinsic ligaments of clinical interest include the scapholunate ligament, the lunotriquetral ligament, and TFCC (►**Fig. 3**). The scapholunate and lunotriquetral ligaments are made of three components: the dorsal and volar components and an interosseous fibrocartilaginous component (►**Fig. 3B**).

Fig. 2 Posteroanterior radiograph of the wrist demonstrating the Gilula arcs. Arc I is drawn through the proximal articular surface of the scaphoid, lunate, and triquetral; arc II is drawn through the distal articular surface of the scaphoid, lunate, and triquetral; and arc III is drawn through the proximal articular surface of the capitate and hamate in the distal carpal row. Note that the pisiform, trapezium, and trapezoid are not a part of the Gilula arcs.

The TFCC is a thick cartilaginous disk that is seen in the ulnocarpal joint space[2] and is a major stabilizer of the DRUJ. The components include the TFC disk proper, dorsal and volar radioulnar ligaments, meniscal homologue, tendon sheath of the extensor carpi ulnaris, ulnar collateral ligament, and the ulnocarpal ligaments (ulnolunate and ulnotriquetral ligaments; ►**Fig. 3C**). The TFC disk proper is a triangular-shaped cartilage that attaches to the ulnar side with a broad base at the fovea (by a proximal lamina) and the base of the styloid process (by the distal lamina). The volar and dorsal components of the ligament are thicker and blend with the radioulnar, ulnocarpal ligaments for reinforcement. The radial attachment is tapered and thinner at the ulnar side of the distal radius. The meniscal homologue is an additional reinforcement at the ulno-dorsal aspect of the TFC between the ulna and the triquetrum. The extensor carpi ulnar tendon sheath also strengthens the TFCC, and the ulnar collateral ligament is very small and often not well visualized on standard MRI.[4] Injuries to the TFCC are a common cause of ulnar-sided pain and instability.

Imaging Modalities

Radiography

Conventional radiography is the first radiological investigation for wrist and hand trauma. It is advisable to have at least three radiographic views in suspected wrist fractures, with a PA view, a lateral view, and an additional semi-pronated 45-degree oblique view[5–7] (►**Fig. 4**). Oblique view demonstrates the waist of the scaphoid and trapezio-trapezoidal joint.[8] Placing the hand in ulnar deviation in the PA position

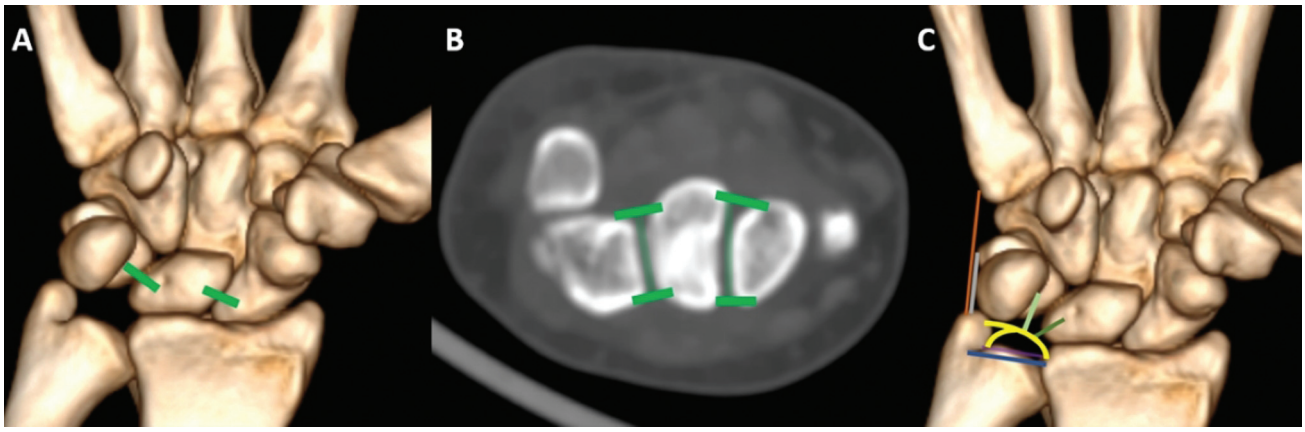

Fig. 3 (**A**, **B**) Scapholunate and lunotriquetral ligaments (*green*) with volar, dorsal, and interosseous components. (**C**) Various components of the triangular fibrocartilaginous complex: articular disk with radial and ulnar attachments (*yellow*); volar (*blue*) and dorsal (*purple*) radioulnar ligaments; ulnolunate (*dark green*) and ulnotriquetral (*light green*) ligaments; ulnar collateral ligament (*gray*) and tendon sheath of the extensor carpi ulnaris tendon (*orange*).

elongates the scaphoid bone, increasing the sensitivity of detecting scaphoid fractures. High-quality radiographs with standardized positioning should be taken for optimal evaluation of wrist injuries. On a standard PA view, the groove for the tendon of the extensor carpi ulnaris should be seen in profile and should be at the level of the base of the ulnar styloid or radial to it. Similarly on a true lateral view, the scaphopisocapitate relationship should be maintained. In the normal wrist, the longitudinal axes of the third metacarpal, capitate, lunate, and distal radius fall in the same line on the lateral view or within 10 degrees of this line (►**Fig. 5**).

Computed Tomography

Quite often, wrist fractures, particularly scaphoid and other carpal injuries, may be radiographically occult. Around 30% of wrist fractures may not be detected on initial radiographs.[9] In patients with a high degree of suspicion of fracture with equivocal or normal radiographs, further imaging with CT without intravenous contrast is warranted.[7,9] In addition, patients having high-impact injuries such as fall from heights or road traffic accidents, those with intra-articular or comminuted fractures, and DRUJ malalignment and carpal dislocations with or without any obvious fracture also require CT for detailed evaluation and operative planning.[10]

Magnetic Resonance Imaging

MRI without intravenous contrast can help in early detection of occult fractures with equivocal radiographic findings. MRI can detect trabecular fractures, which are overlooked on CT. Additionally, it is useful for detecting tendon, ligament, muscle, and soft tissue injuries. In occult scaphoid fractures, a short protocol MRI may be performed in the emergency room.[11] Optimized parameters for MRI of the wrist include an appropriate field of view (8–12 cm) with a slice thickness of 3 mm.[12] The use of dedicated phased-array extremity coils improves the resolution of the study. Fast spin echo sequences in two dimensions such as T2-weighted or proton density with fat suppression in all three orthogonal planes are ideal for detecting bone marrow edema and fracture lines. T1-weighted sequences are also added for bony alignment and fracture line detection.

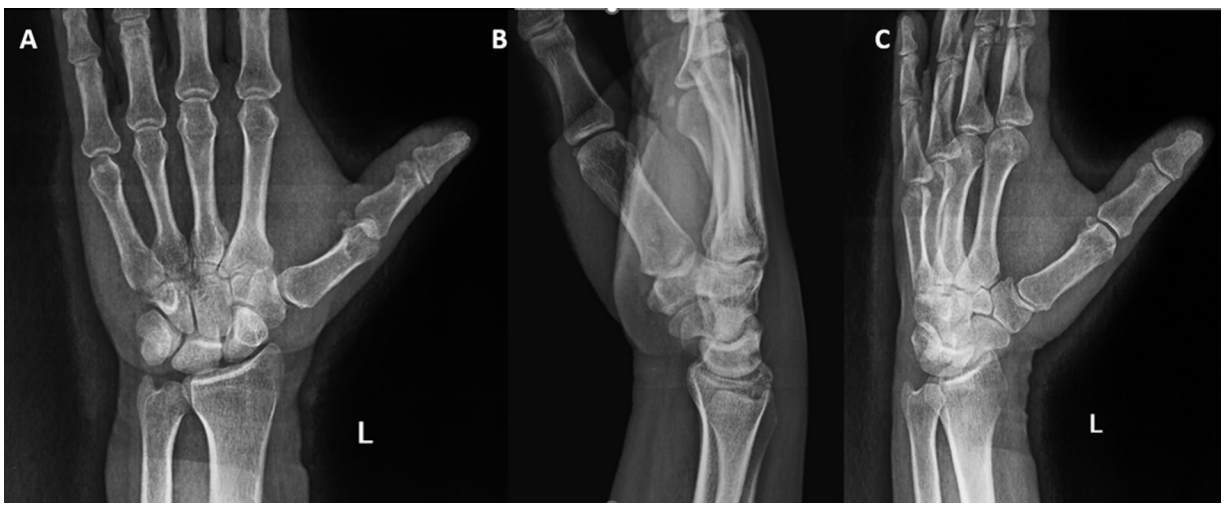

Fig. 4 Standard radiographic views of the wrist: (**A**) posteroanterior, (**B**) lateral, and (**C**) oblique views.

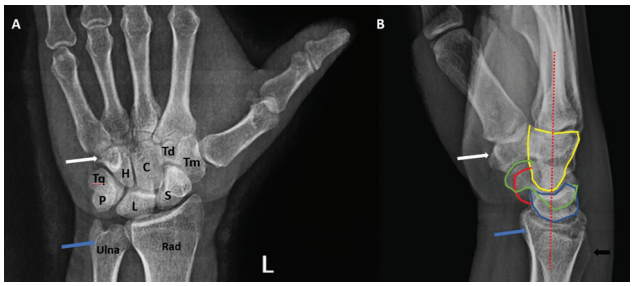

Fig. 5 Normal anatomy on posteroanterior (PA) and lateral views. (**A**) PA radiograph showing all the carpal bones, distal radius, and ulna. Also note the hook of the hamate (*white arrow*), which is seen as a ring-like structure on the PA view. In the optimal PA view, the groove for the extensor carpi ulnaris tendon should be seen in the profile (*blue arrow*). (**B**) Lateral view showing the capitate (*yellow*), lunate (*blue*), scaphoid (*green*), pisiform (*red*), trapezium (*white arrow*), distal radius (*blue arrow*), and ulna (*black arrow*). In the true lateral view, the palmar cortex of the pisiform should lie between the palmar cortices of the scaphoid and the capitate. Also note the normal relationship between the capitate, lunate, and radius (*dashed red line*).

Distal Radius Fractures

Distal radius fractures (DRFs) are the commonest fractures around the wrist joint, with high incidence in all age groups.[13] They are important in the geriatric population where the eponymous Colles' fracture is common in the setting of osteoporosis. Many of the eponymous DRFs are commonly used, although the use of eponyms should be discouraged in favor of more clinically relevant and reproducible classification systems. However, radiologists should be familiar with the various fracture eponyms as they are commonly used in clinical practice. Colles' fracture is a transverse DRF without intra-articular extension and dorsal displacement or angulation of the fracture fragment (►**Fig. 6A, B**). It is typically caused by a fall on outstretched hand while the wrist is dorsiflexed. Smith's fracture (reverse Colles' fracture) is a transverse, extra-articular fracture of the distal radius with volar displacement or angulation of the fracture fragment (►**Fig. 6C, D**), and results from high-energy trauma on palmar flexed wrists in the younger population. A Barton's fracture is an intra-articular fracture of the distal radius with displacement of the fracture fragment and carpus (►**Fig. 6E, F**). It implies a shear pattern of injury. The volar and dorsal Barton fractures are distinguished by the location of the fracture and the direction of displacement. A Hutchison fracture (also known as chauffeur's fracture) is an oblique fracture of the radial styloid with intra-articular extension[8] (►**Fig. 6G**).

Several classification systems exist for DRFs. The most commonly used current classification systems for DRFs are the AO, Fernandes, and Frykman classifications.[14] However, studies have shown that the commonly applied fracture classifications are not universally reproducible on radiographs or CT, and therefore not used as standard methods of classification.[15,16] The most important considerations for assessing severity of radial fractures are the following: displacement of the fracture fragments, intra-articular extension of fracture with intra-articular step-off (DRUJ or radiocarpal joint), and the presence of comminuted fragments and associated ulnar or other carpal bone and soft tissue injuries.

Fig. 6 Posteroanterior and lateral radiographs of the wrist in different patients demonstrating (**A, B**) Colle's fracture (*blue arrow*), (**C, D**) Smith's fracture (*blue arrow*), and (**E, F**) volar Barton's fracture (*blue arrow*). (**G**) Oblique radiograph of the wrist demonstrating a fracture of the radial styloid (*blue arrow*) suggestive of a Hutchinson fracture. Also note the coexisting fractures of the ulnar styloid (*white arrow*) and the hamate (*black arrow*).

Fig. 7 (A) Lateral radiograph of the wrist showing a normal pronator quadratus fat stripe (*white arrow*). (B) Extra-articular fracture of the distal radius with obliteration of the pronator quadratus fat stripe.

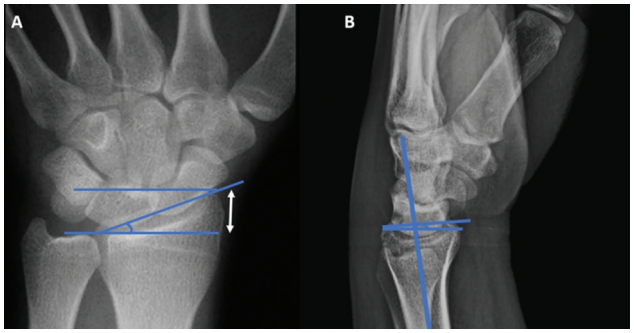

Fig. 8 Distal radius measurements on radiograph. (A) On posteroanterior view: radial length is the distance between the tip of the radial styloid and the ulnar articular surface (*white arrow*). Radial inclination is the angle between two lines drawn through the distal articular surface of the radius and a line drawn perpendicular to the long axis of the radius. (B) On lateral view: radial tilt is the angle between lines drawn through the distal articular surface and the line drawn perpendicular to mid-shaft of the radius.

Radiographs in suspected DRFs should be carefully evaluated for any cortical discontinuity. Associated soft tissue swelling and obliteration of the pronator quadratus fat stripe (►**Fig. 7**) may provide a clue to the diagnosis in subtle fractures. The dorsal rim of the distal radius is always smooth and without any bumps or step-offs. The presence of a slight irregularity or a dorsal osseous bump is a subtle indicator of an impacted or minimally displaced DRF. Radiographic assessment of the DRFs should include three measurements that correlate with long-term patient outcome. On PA radiographs, one should evaluate for the *radial length* (to evaluate for radial foreshortening) and radial inclination (►**Fig. 8A**). To measure radial length, two perpendicular lines to the long axis of the radius are drawn, one at the tip of the radial styloid and one at the tip of the radial aspect of the DRUJ, and the distance is measured. Normal radial length ranges from 11 to 22 mm. Excessive radial foreshortening can predispose to TFCC injury and ulnar impaction injuries. *Radial inclination* refers to the angle between a line joining the lateral and medial radial tips and perpendicular to the long axis of the radius. The normal angle is between 13 and 30 degrees.[17] On the lateral view, one should inspect for volar or dorsal tilt of the radius (►**Fig. 8B**). Normal range for radial tilt is from 4 degrees of dorsal tilt to 11 degrees of volar tilt. Most DRFs are accompanied by loss of the normal volar flexion of the distal radius. In addition to these three measurements, one should also look for ulnar variance on PA radiograph, which will be positive in case of radial shortening (►**Fig. 9**). A decrease in radial length by more than 2 mm, dorsal tilt of radius by more than 20 degrees, and radial inclination by less than 10 degrees is associated with decreased wrist function in the long term[8] (►**Fig. 10**).

The use of CT better demonstrates the details and extent of DRFs with 3D volume rendering and multiplanar evaluation allowing for planning the most appropriate management and preoperatively assessing the outcome.[18,19] Fracture displacement, comminution, and intra-articular step-off can be better demonstrated on CT (►**Fig. 11**). It has been shown that an articular step-off greater than 2 mm is associated with late development of osteoarthritis in a significant number of patients and warrants open reduction and internal fixation.[8] The association with carpal injuries (like associated scaphoid injuries—often radiographically occult) also makes CT useful as it can detect very subtle

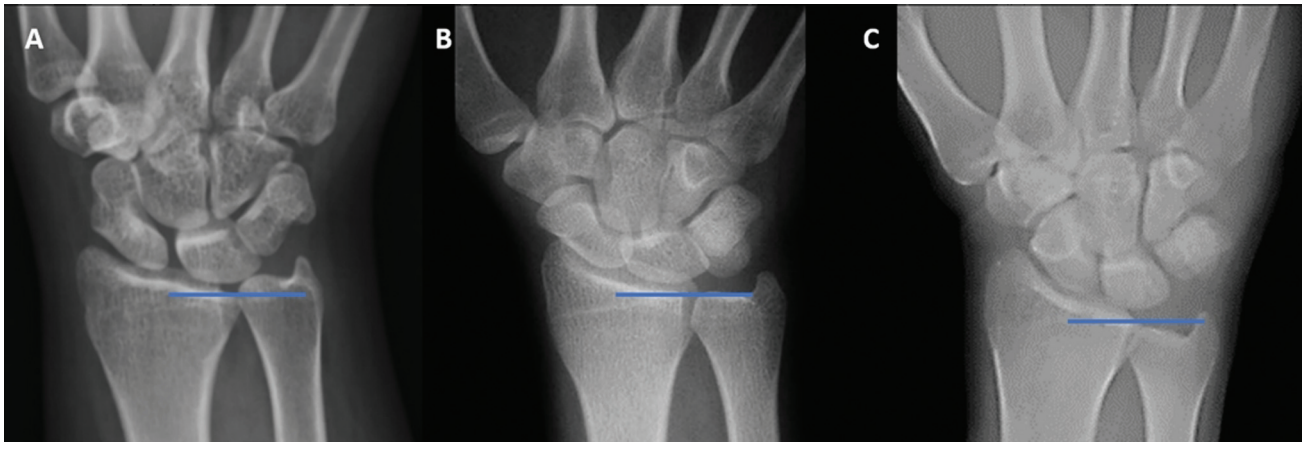

Fig. 9 Posteroanterior radiographs of the wrist in different patients showing (A) positive, (B) neutral, and (C) negative ulnar variance.

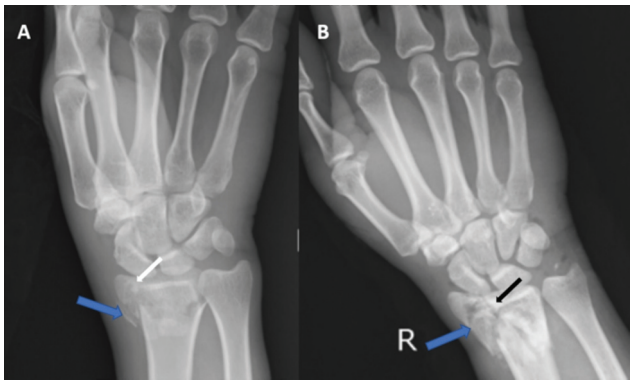

Fig. 10 (A) Posteroanterior (PA) radiograph of the wrist demonstrating a comminuted fracture of the distal radius (*blue arrow*) with intra-articular extension (*white arrow*) and loss of the radial length and inclination. (**B**) PA radiograph in another patient demonstrating a comminuted fracture of the distal radius (*blue arrow*) with intra-articular extension (*black arrow*). The radial length and inclination are, however, preserved.

nondisplaced scaphoid fractures.[9,20] MRI can detect radiographically occult trabecular injuries without cortical breech (►**Fig. 12**). In children, acute fractures commonly involve radial and ulnar physis.[17] Torus fractures are not uncommon in younger children and appear as incomplete fractures with cortical bulge (►**Fig. 13**).

Distal Ulna Fractures

Distal ulna fractures mostly occur in concurrence with DRFs. The clinical outcome of these fractures largely depends on the severity and management of the DRF. Most commonly, it is the ulnar styloid that is associated with DRFs, and the Frykman classification for DRFs includes a subgroup in each stage to include ulnar styloid fracture. Most of the ulnar styloid fractures are in the tip of the ulna (<2 mm along its length); more proximal fractures involving the base of the styloid (►**Fig. 14**) and those with intra-articular extension are often associated with DRUJ dislocation and instability.

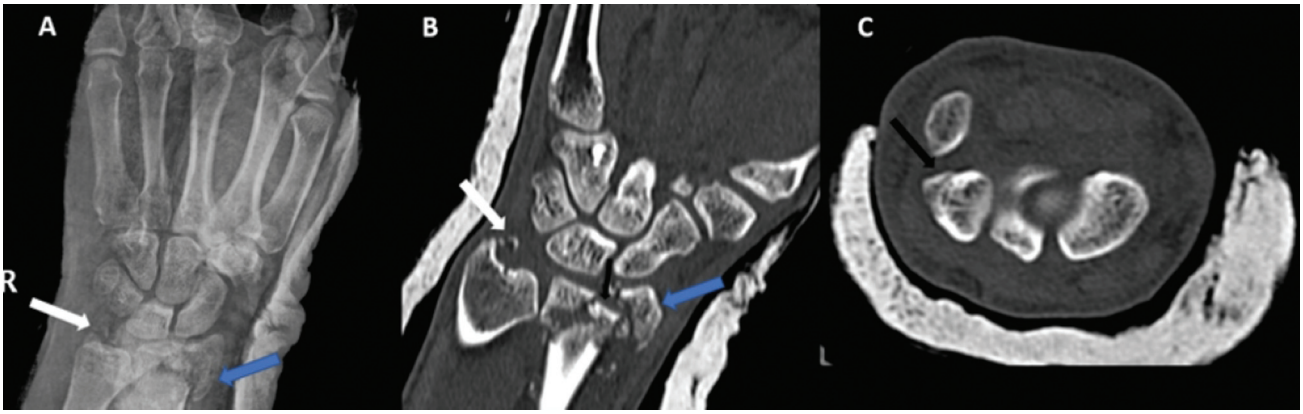

Fig. 11 (A) Posteroanterior radiograph of the wrist demonstrating a comminuted fracture of the distal radius (*blue arrow*) with suspicious intra-articular extension. Also note the associated fracture of the ulnar styloid (white arrow). (**B**) Coronal computed tomography image showing an extensively comminuted intra-articular fracture of the distal radius with articular step-off (*black arrow*), which was not seen on radiograph. (**C**) Also note the associated fracture of the triquetral (*black arrow*) missed on radiograph.

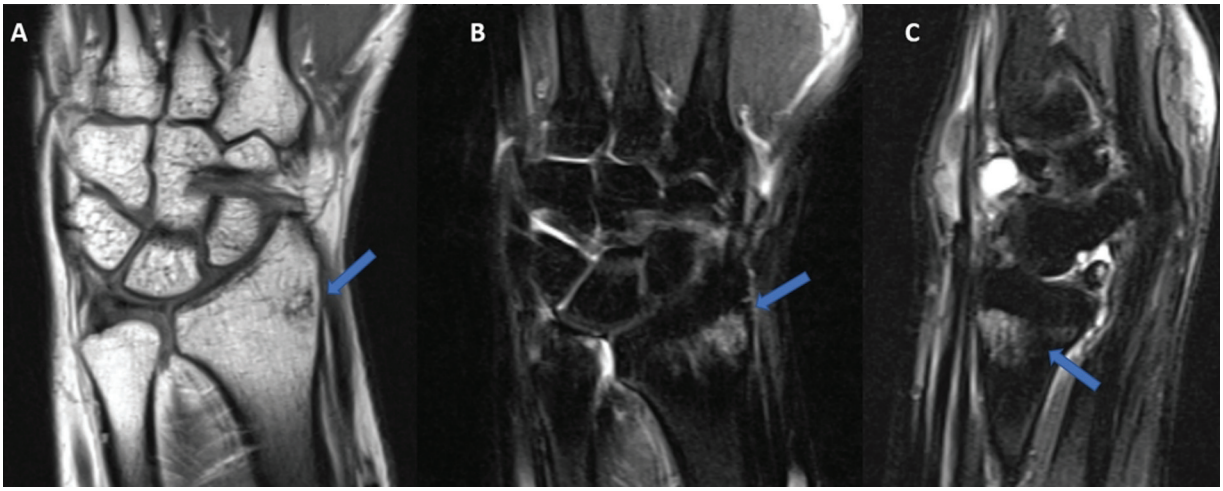

Fig. 12 (A) T1-weighted (T1W) coronal, (**B**) T2W coronal fat-saturated, and (**C**) proton density fat-saturated sagittal images demonstrating a hypointense fracture line in the distal radius (*blue arrow* in **A**) with adjacent marrow edema (*arrows* in **B** and **C**). The fracture was occult on radiograph.

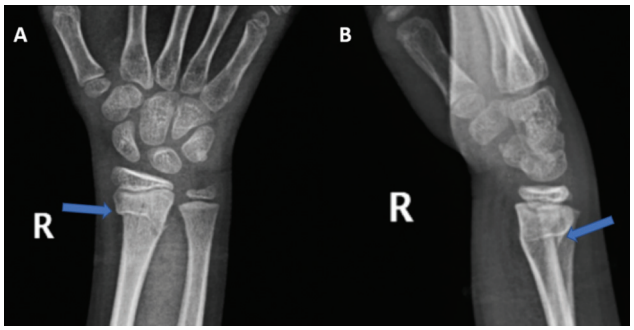

Fig. 13 (A) Posteroanterior and (B) lateral radiographs of the wrist in a child demonstrating a torus fracture of the distal radius (*blue arrow*) with involvement of the lateral cortex.

Isolated ulnar head fractures also occur, and although they are relatively uncommon, they are usually unstable fractures.[21]

It is important to assess for DRUJ instability in the presence of both bone fractures and extensively comminuted wrist injuries.[1] On the PA view, there may be widening of the radioulnar interval, foreshortening of the radius, as well as fracture extending into the sigmoid notch of the radius. On a radiographic true lateral view, a distance of more than 6 mm between the dorsal cortices of the radius and the ulna indicates DRUJ instability.[22] The caveat is that the radiograph must be acquired in true lateral position, and even minimal rotation can lead to false interpretation. CT is considered the standard investigation to evaluate for DRUJ dislocations. The three common methods for evaluating DRUJ instability on CT are the Mino method[23] (measurement of the radioulnar line on axial scan), the congruency method,[24] and the epicenter method.[25] Currently, the epicenter method is preferred because of the high false-positive rates of the other two techniques.[25] In the epicenter method, a line is drawn joining the ulnar styloid and the center of the ulnar head. The midpoint of this line represents the center of the DRUJ axis. Another line along the sigmoid notch of the distal radius is drawn. A perpendicular from this line is drawn to the center of the DRUJ axis. In the stable DRUJ, the perpendicular line lies in the middle of the sigmoid notch (►**Fig. 15**).

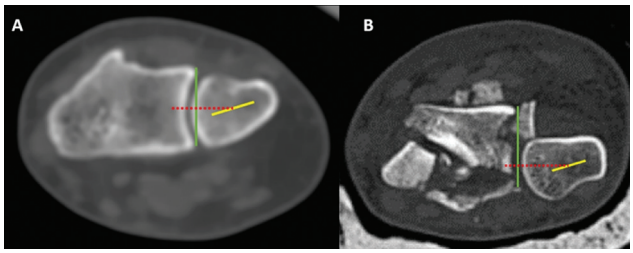

Fig. 15 Epicenter method for the distal radioulnar joint (DRUJ) instability in (**A**) a stable and (**B**) subluxated DRUJ. A line is drawn through the center of the ulnar head and the styloid (*yellow line*), and another line through the sigmoid notch (*green line*). A line perpendicular to the sigmoid notch (*dashed red line*) is then drawn from the center of this line. In a stable DRUJ, this perpendicular lies in the middle of the sigmoid notch (**A**).

Carpal Fractures

The most common carpal bone fracture is that of the scaphoid. It is commonly seen in young adults and sportspersons who fall on an outstretched hand.[26] In spite of being a common injury, it is often overlooked on radiographs due to its complex anatomy, and subtle minimally displaced fracture lines. The scaphoid is anatomically divided into a waist, proximal pole, and distal pole. A complication of scaphoid fractures is nonunion and osteonecrosis due to the tenuous blood supply of the bone. The main vascular supply is from a dorsal artery, which extends from the waist to the proximal pole.[27] An additional vascular supply is from a palmar artery that supplies the distal pole. The proximal pole therefore receives its supply through the waist of the scaphoid, and therefore avascular osteonecrosis is more common in proximal pole fractures and those with a high degree of comminution.[28] The suggested radiographic views for suspected scaphoid fracture comprises four views:

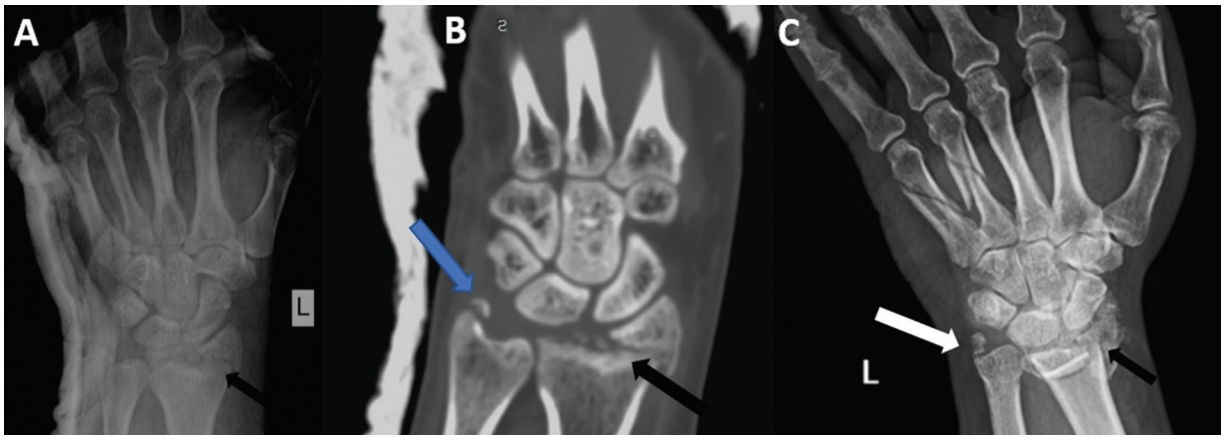

Fig. 14 (**A**, **B**) Fracture of the tip of the ulnar styloid. Coronal reformatted computed tomography (CT) image showing a fracture of the tip of the ulnar styloid (*blue arrow*), which was not appreciated on radiograph (**A**). Also note the associated distal radial fracture (*black arrow*). (**C**) Fracture base of the ulnar styloid. PA radiograph of the wrist showing fracture of base of the ulnar styloid (*white arrow*) with an associated comminuted fracture of the distal radius (*black arrow*). Also note the poorly visualized hook of the hamate with fractures of the fourth and fifth metacarpals. The fracture of the hook of the hamate was present on CT (not shown here).

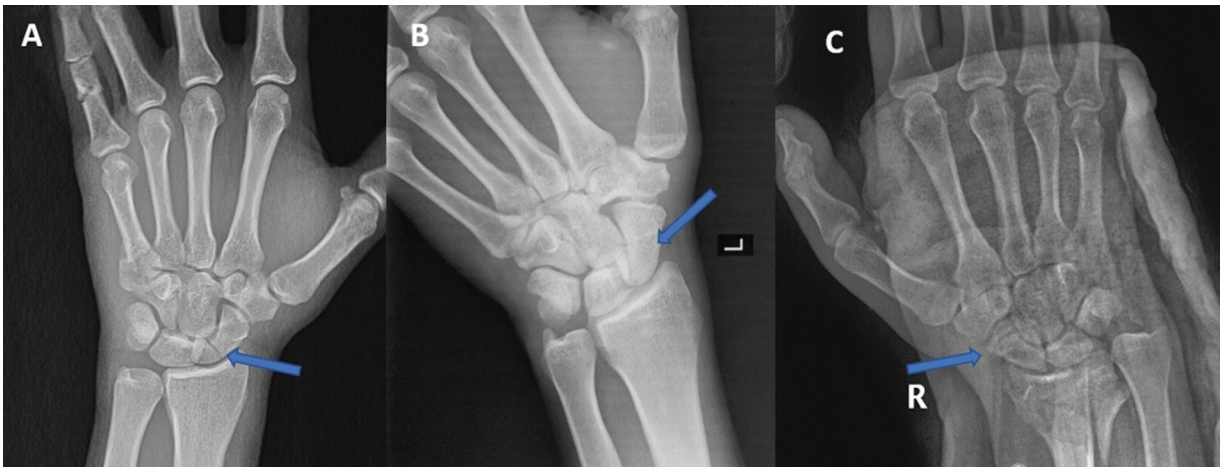

Fig. 16 Posteroanterior radiographs of the wrist in three different patients demonstrating fractures of the scaphoid through (**A**) the proximal pole (*blue arrow*), (**B**) waist (*blue arrow*), and (**C**) distal pole (*blue arrow*).

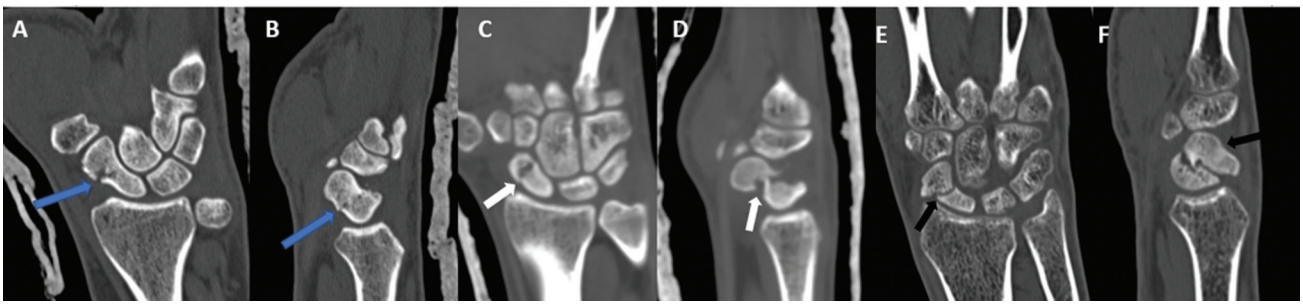

Fig. 17 Coronal and sagittal reformatted images in three different patients depicting (**A, B**) a minimally displaced fracture through the waist of the scaphoid without significant angulation (*blue arrow*), (**C, D**) displaced fracture through the scaphoid waist with volar angulation of the proximal fracture fragment (*white arrow*), and (**E, F**) displaced fracture through the scaphoid waist with significant volar angulation of the proximal and distal fracture fragments resulting in humpback deformity (*black arrow*).

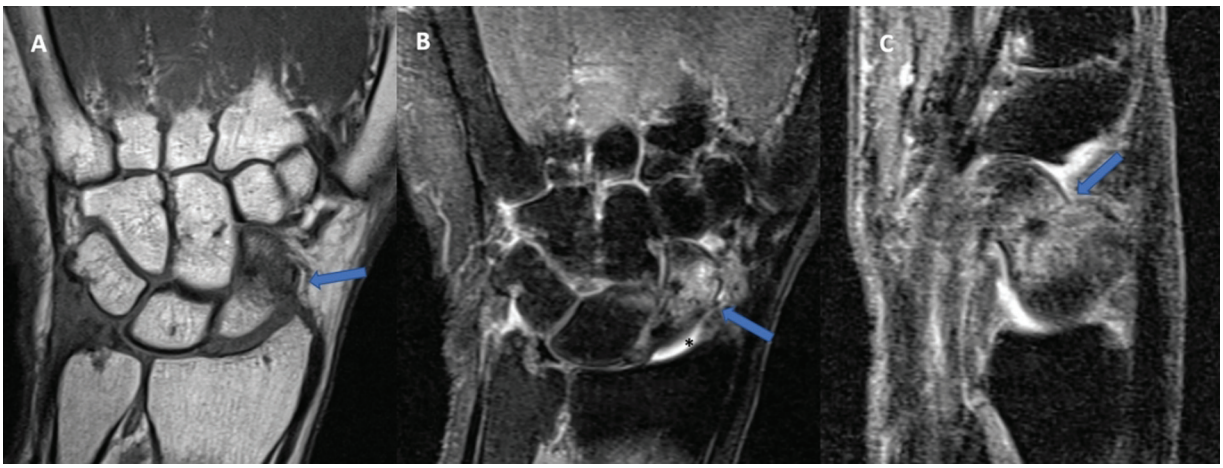

Fig. 18 (**A**) T1-weighted (T1W) coronal, (**B**) T2W coronal fat-saturated, and (**C**) proton density fat-saturated sagittal images demonstrating a hypointense fracture line through the waist of the scaphoid (*blue arrow*) with an adjacent marrow edema.

PA and lateral views and pronated oblique and PA views with ulnar deviation are additionally used to detect the fracture.[29] Fracture lines can be seen in undisplaced scaphoid fractures with interruption of the cortex (►**Figs. 16** and **17**). The scaphoid fat stripe may be obliterated in occult scaphoid fractures. A sizable proportion of the occult scaphoid fractures may be missed on initial radiography, and in such patients, CT has utility in detected scaphoid fractures with high sensitivity and specificity.[30] MRI can also demonstrate radiographically occult scaphoid fractures, particularly trabecular fractures (►**Fig. 18**); however, availability, long examination time, and cost remain the limiting factors.

According to the Mayo clinic classification, scaphoid fractures are classified based upon the anatomic location:

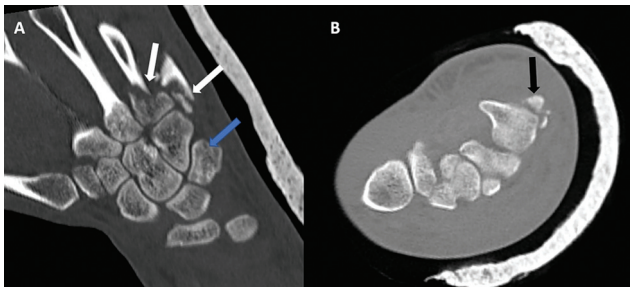

Fig. 19 (A) Coronal reformatted and (B) axial computed tomography images show fractures of the triquetrum (*blue arrow*) and hamate (*black arrow*). Also note the associated fractures of the base of the fourth and fifth metacarpals (*white arrow*).

proximal pole, waist, distal pole, scaphoid tuberosity, and distal articular surface. Fractures of the waist are most common (comprising 80% scaphoid fractures) followed by proximal pole[3] (►**Fig. 16**). Scaphoid fractures with displacement, comminution, and obliquity are mechanically unstable (►**Fig. 17**).

The second most common carpal bone fracture is the triquetral fracture (►**Figs. 11** and **19**). Together the triquetral and scaphoid fractures greatly outnumber other carpal bone fractures.[17] The majority of the triquetral fractures occur on the dorsal surface due to impaction from the ulnar styloid in hyperextension injuries or due to avulsion of the ligamentous attachment in hyperflexion injuries. These fractures are best detected on the oblique or lateral view.

Lunate fractures are difficult to identify on radiographs due to considerable overlap from surrounding bones. These fractures are less common; however, like scaphoid fractures, they are at a risk of avascular necrosis if left untreated. They are also associated with carpal instability and dislocations (discussed later in the text). On the lateral view, careful evaluation of the dorsal and volar cortices of the lunate should be done. The finding of the perilunate subluxation or dislocation on lateral views may also suggest an associated lunate injury.[17] CT is helpful in detecting radiographically occult fractures (►**Fig. 20**).

In the distal carpal row, the hamate may be fractured. The most common pattern of hamate injury is fracture of the hook of the hamate, commonly seen in athletes.[26,31] The hook of the hamate is a projection on the palmar surface of the hamate, and its fracture may be difficult to identify on PA radiographs. Absence of the hook or indistinct margins on PA radiographs can point toward a fracture[32] (►**Fig. 21**). A carpal tunnel radiograph is used to demonstrate fractures of the hook of the hamate,[32] and alternatively CT confidently demonstrates the fracture in all cases. One must be aware of an anatomical variant of the hamate, which is the bipartite hamate, or *os Hamuli proprium*, which is present due to failure of fusion of the hook of the hamate and can be misdiagnosed as a fracture. Neglected hook of the hamate fractures are prone to nonunion, osteonecrosis, or impingement of the ulnar nerve in Guyon's canal. Fractures of the body of the hamate may also occur (►**Figs. 19** and **22**), and these are commonly associated with fractures of the fourth and fifth metacarpal bases and the fourth and fifth carpometacarpal dislocations.

Pisiform fractures are less common, and result from a fall on the outstretched hand[31] (►**Fig. 23**). Avulsion fractures of the pisiform can be seen due to the strong ligaments and muscular tendon (flexor carpi ulnaris), which invest the bone. Fractures of the trapezium occur at the trapezial ridge, along the articular surface with the first metacarpal base. These fractures are associated with the first carpometacarpal injuries, and are frequently intra-articular. Fractures of trapezoid are very rare and usually occur in association with other carpal fractures (►**Fig. 21**). The capitate is the largest carpal bone and is injured in high-energy hyperextension force (►**Fig. 24**). Capitate fractures are usually transverse in orientation.[3]

Carpal Dislocations

These are high-velocity traumatic injuries resulting in severe disruption of the alignment of the carpus with

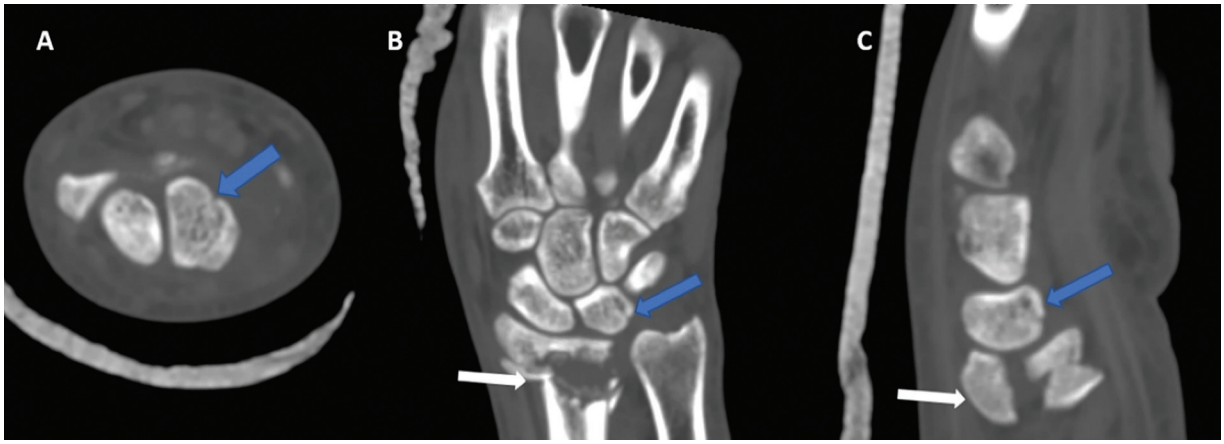

Fig. 20 (A) Axial, (B) coronal, and (C) sagittal reformatted images demonstrate a linear undisplaced fracture of the lunate (blue arrow). Also note the comminuted fracture involving the distal radius (*white arrow*).

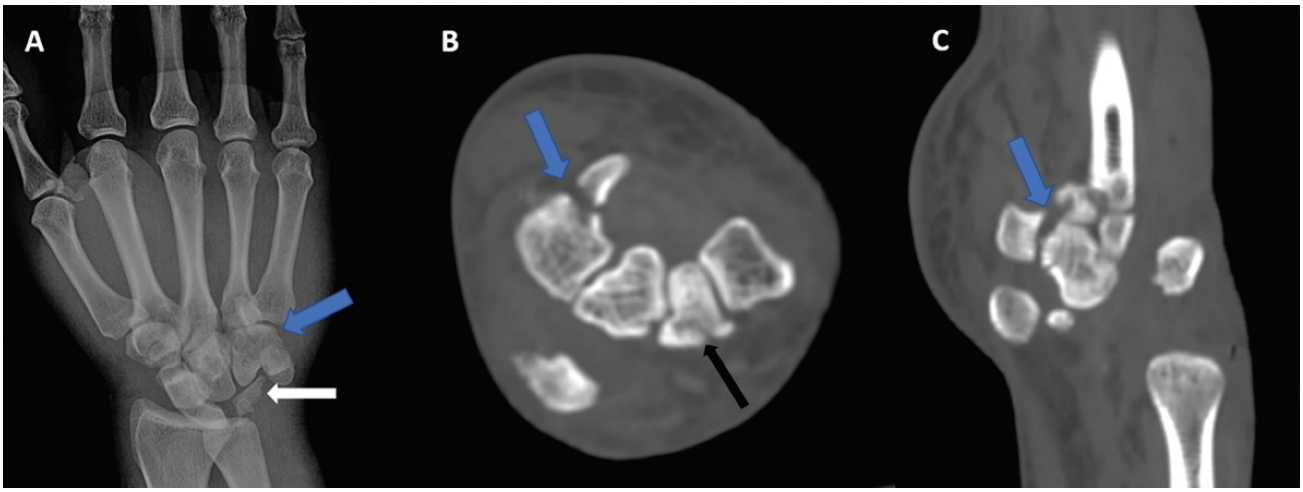

Fig. 21 (**A**) The hook of the hamate is not visualized on the posteroanterior radiograph of the wrist (*blue arrow*). (**B**) Axial and (**C**) sagittal reformatted computed tomography (CT) images demonstrate a fracture of the hook of the hamate (*blue arrow*). Also note the fracture dislocations involving the proximal carpal row (*white arrow* in **A**) and undisplaced fracture involving the trapezoid (*black arrow* in **B**). On CT, fractures were also seen involving the triquetrum and the scaphoid with an associated midcarpal dislocation (not shown here).

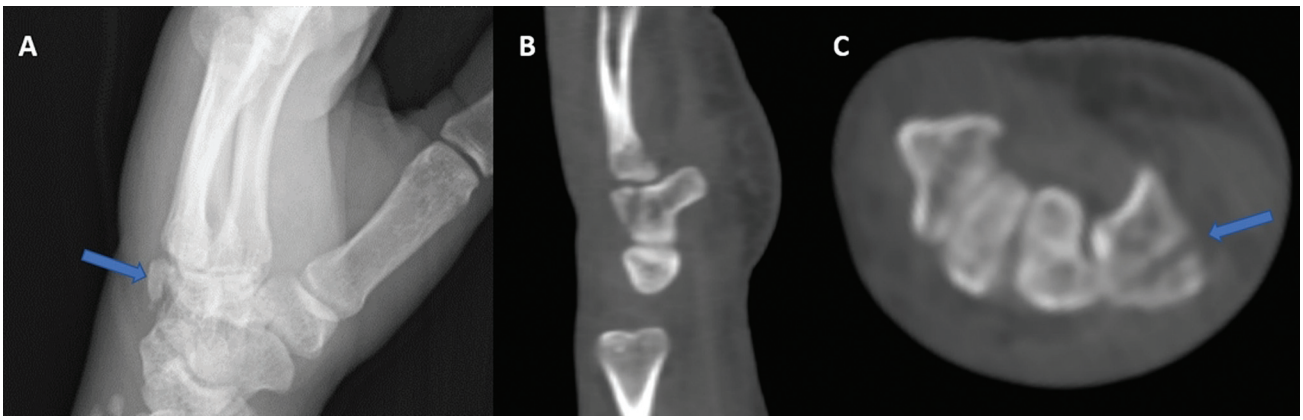

Fig. 22 (**A**) Oblique radiograph, (**B**) sagittal reformatted, and (**C**) axial computed tomography images showing a fracture through the dorsal surface of the hamate (blue arrow).

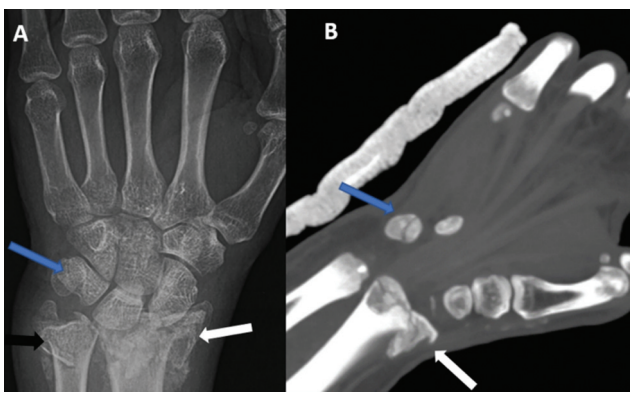

Fig. 23 (**A**) Posteroanterior radiograph and (**A**) coronal computed tomography image showing a fracture of the pisiform (*blue arrow*). Also note the presence of the comminuted fractures of the distal radius (*white arrow*) and ulna (*black arrow*).

associated soft tissue injury and bony fractures. The most common of these is perilunate instability.[33] According to Mayfield et al, there are four stages of progression of a perilunate dislocation.[34] Stage I is scapholunate dissociation, marked by disruption of the scapholunate ligament with resultant widening of the interval (also called as lesser arc injury with mainly soft tissue and ligamentous disruption). Stage II is perilunate dislocation (►**Fig. 25B**), wherein the lunate remains aligned with the distal radius, but the surrounding carpus is dislocated (mostly dorsally) with disruption of the capitolunate ligament and joints (greater arc injuries with involvement of multiple carpal bones such as trans-scaphoid perilunate dislocation). Stage III results from lunotriquetral joint disruption with tear of the radiotriquetral ligaments. In the final stage IV, there is disruption of the radiolunate ligaments releasing the lunate bone, which is then free to displace along the palmar surface (►**Fig. 25C**).

Perilunate dislocations can occur with or without an associated fracture. When associated with a fracture, these injuries are termed as greater arc injuries and are twice as frequent as lesser arc injuries (dislocation without associated fracture). Trans-scaphoid perilunate dislocation is the most common pattern of perilunate fracture dislocation (►**Fig. 26**). Radiographic findings on PA view include

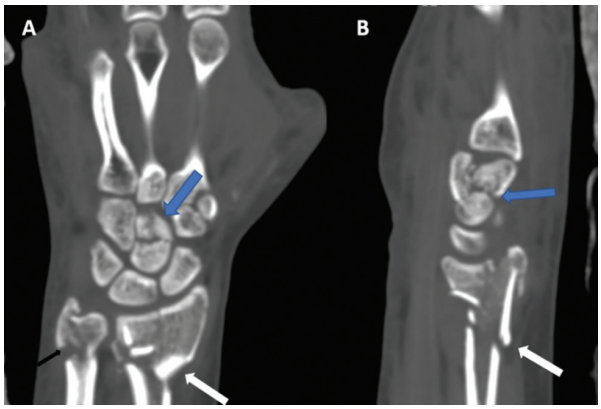

Fig. 24 (A) Coronal and (B) sagittal reformatted images showing a comminuted fracture of the capitate (*blue arrow*). Also note the comminuted fractures of the distal radius (*white arrow*) and ulna (*black arrow*).

scaphoid fracture, triangular appearance of the lunate, and disruption of the carpal arcs. Widening of the scapholunate interval on the PA view indicates a scapholunate ligament injury and is an early sign of perilunate dislocation. On lateral view, alignment of the distal radius and lunate is maintained with dorsal dislocation of the capitate. Lunate dislocation is the final stage of the perilunate injury and is highly unstable. It is characterized by volar dislocation of the lunate on lateral radiograph (known as "spilled tea-cup sign") with maintained alignment between the distal radius and the rest of the carpus (►**Figs. 25** and **27**). In addition to perilunate and lunate dislocations, midcarpal dislocations are another group of carpal dislocations characterized by loss of alignment between the distal radius, lunate, and capitate (►**Figs. 25** and **28**). On lateral view, there is dorsal subluxation of the capitate with volar subluxation of the lunate. They are considered a variant of stage III perilunate dislocations.[33]

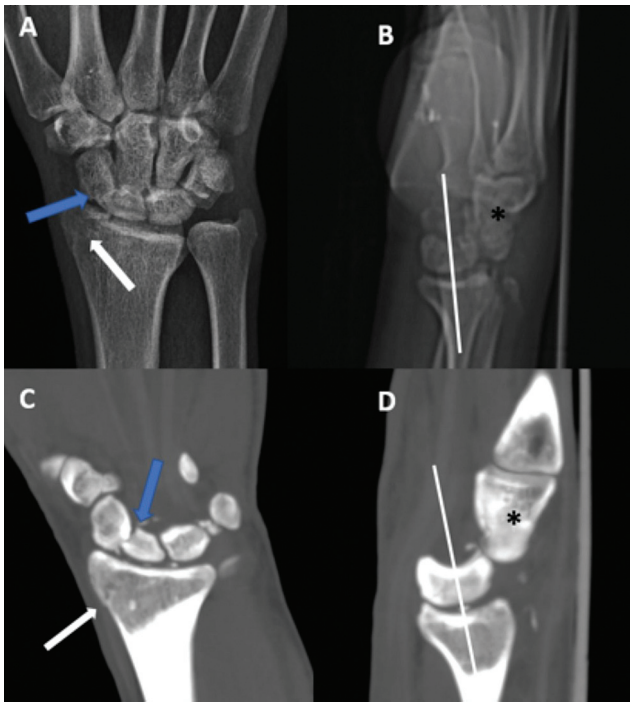

Fig. 26 Trans-scaphoid fracture dislocation. (A) Posteroanterior radiograph of the wrist showing a displaced fracture through the waist of the scaphoid (blue arrow). (B) Lateral radiograph demonstrating a perilunate dislocation where alignment of the radius with the lunate is maintained (white line) with a posterior dislocation of the capitate (*). Coronal (C) and Sagittal (D) reformatted CT images confirm the findings. Also note the undisplaced fracture through the radial styloid (white arrow).

Conclusion

Wrist fractures and dislocations are common yet complex entities. Prompt and accurate diagnosis allows for adequate management and aids in surgical planning. Thorough knowledge of wrist anatomy, normal imaging appearance, and

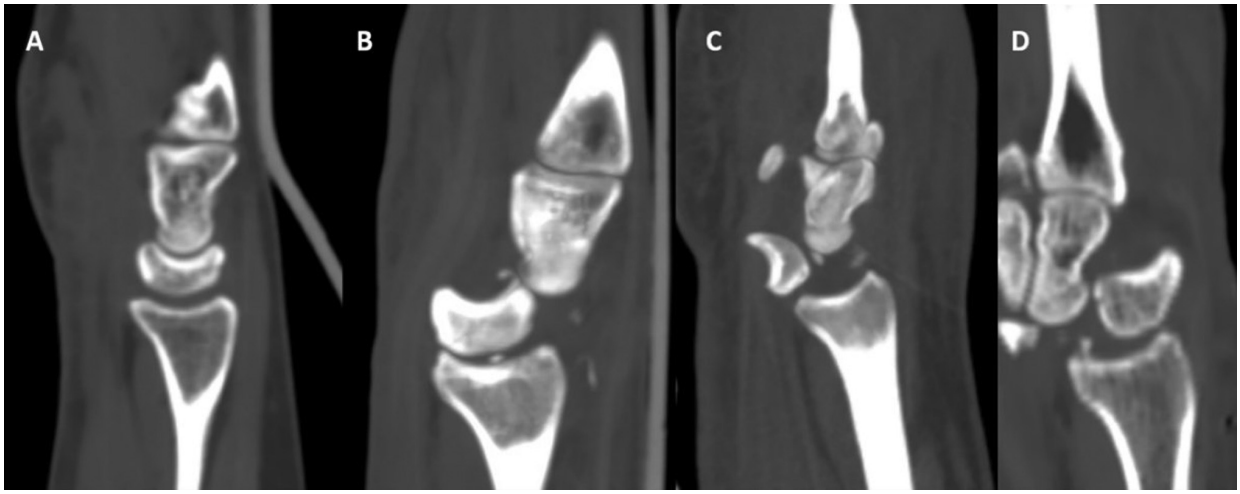

Fig. 25 Sagittal reformatted computed tomography images showing alignment of the capitate, lunate, and radius in (A) normal case, (B) perilunate dislocation, (C) lunate dislocation, and (D) midcarpal dislocation. In the perilunate dislocation, alignment between the radius and the lunate is maintained, while in the lunate dislocation (B), alignment between the radius and the capitate is maintained (C). In the midcarpal dislocation, alignment between all three bones is lost (D).

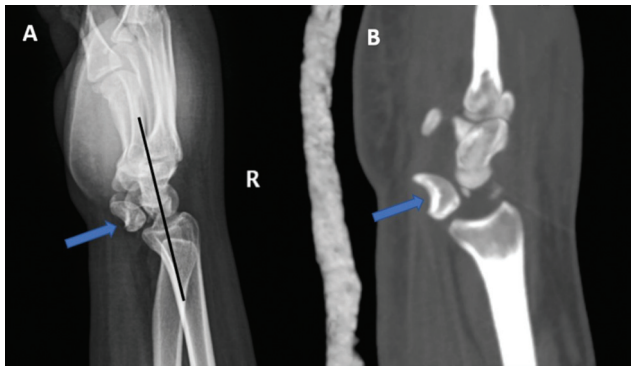

Fig. 27 (**A**) Lateral radiograph and (**B**) sagittal reformatted computed tomography image showing a lunate dislocation (*blue arrow*) with a "spilled tea-cup" sign.

Fig. 28 Lateral radiograph of the wrist showing a midcarpal dislocation with complete loss of alignment between the distal radius (*), lunate (*blue arrow*), and capitate (*).

various injury patterns is necessary for complete radiological evaluation. We have illustrated various common wrist fractures and dislocations that one can come across in the emergency department.

Funding
None.

Conflict of Interest
None declared.

References

1 Squires JH, England E, Mehta K, Wissman RD. The role of imaging in diagnosing diseases of the distal radioulnar joint, triangular fibrocartilage complex, and distal ulna. AJR Am J Roentgenol 2014;203(01):146–153
2 van der Post AS, Jens S, Smithuis FF, Obdeijn MC, Oostra RJ, Maas M. The triangular fibrocartilage complex on high-resolution 3 T MRI in healthy adolescents: the thin line between asymptomatic findings and pathology. Skeletal Radiol 2021;50(11):2195–2204
3 Kaewlai R, Avery LL, Asrani AV, Abujudeh HH, Sacknoff R, Novelline RA. Multidetector CT of carpal injuries: anatomy, fractures, and fracture-dislocations. Radiographics 2008;28(06):1771–1784
4 Bateni CP, Bartolotta RJ, Richardson ML, Mulcahy H, Allan CH. Imaging key wrist ligaments: what the surgeon needs the radiologist to know. AJR Am J Roentgenol 2013;200(05):1089–1095
5 Gilbert TJ, Cohen M. Imaging of acute injuries to the wrist and hand. Radiol Clin North Am 1997;35(03):701–725
6 De Smet AA, Doherty MP, Norris MA, Hollister MC, Smith DL. Are oblique views needed for trauma radiography of the distal extremities? AJR Am J Roentgenol 1999;172(06):1561–1565
7 American College of Radiology. ACR Appropriateness Criteria®. Acute Hand and Wrist Trauma. Reston, VA: ACR; 2018
8 Goldfarb CA, Yin Y, Gilula LA, Fisher AJ, Boyer MI. Wrist fractures: what the clinician wants to know. Radiology 2001;219(01):11–28
9 Welling RD, Jacobson JA, Jamadar DA, Chong S, Caoili EM, Jebson PJL. MDCT and radiography of wrist fractures: radiographic sensitivity and fracture patterns. AJR Am J Roentgenol 2008;190(01):10–16
10 Wieschhoff GG, Sheehan SE, Wortman JR, et al. Traumatic finger injuries: what the orthopedic surgeon wants to know. Radiographics 2016;36(04):1106–1128
11 Kumaravel M, Weathers WM. Emergency magnetic resonance imaging of musculoskeletal trauma. Magn Reson Imaging Clin N Am 2016;24(02):391–402
12 Vassa R, Garg A, Omar IM. Magnetic resonance imaging of the wrist and hand. Pol J Radiol 2020;85:e461–e488
13 Porrino JA Jr, Maloney E, Scherer K, Mulcahy H, Ha AS, Allan C. Fracture of the distal radius: epidemiology and premanagement radiographic characterization. AJR Am J Roentgenol 2014;203(03):551–559
14 Shehovych A, Salar O, Meyer C, Ford DJ. Adult distal radius fractures classification systems: essential clinical knowledge or abstract memory testing? Ann R Coll Surg Engl 2016;98(08):525–531
15 Belloti JC, Tamaoki MJS, Franciozi Cda S, et al. Are distal radius fracture classifications reproducible? Intra and interobserver agreement. Sao Paulo Med J 2008;126(03):180–185
16 Arealis G, Galanopoulos I, Nikolaou VS, Lacon A, Ashwood N, Kitsis C. Does the CT improve inter- and intra-observer agreement for the AO, Fernandez and Universal classification systems for distal radius fractures? Injury 2014;45(10):1579–1584
17 Loredo RA, Sorge DG, Garcia G. Radiographic evaluation of the wrist: a vanishing art. Semin Roentgenol 2005;40(03):248–289
18 Gong XY, An GS, Gao ZQ, Li SL, Rong GW. The role of CT in the diagnosis and treatment of distal radius fracture. Zhonghua Wai Ke Za Zhi 2006;44(20):1414–1416
19 Amin MM, Abdel Wahab MA, Sadek AF, Gomaa BMA. Role of multidetector computed tomography (MDCT) with MPR in assessment of fracture patterns around the wrist join. Minia Journal of Medical Research. 2020;31(04):101–109
20 Balci A, Basara I, Çekdemir EY, et al. Wrist fractures: sensitivity of radiography, prevalence, and patterns in MDCT. Emerg Radiol 2015;22(03):251–256
21 Logan AJ, Lindau TR. The management of distal ulnar fractures in adults: a review of the literature and recommendations for treatment. Strateg Trauma Limb Reconstr 2008;3(02):49–56
22 Nakamura R, Horii E, Imaeda T, Tsunoda K, Nakao E. Distal radioulnar joint subluxation and dislocation diagnosed by standard roentgenography. Skeletal Radiol 1995;24(02):91–94
23 Mino DE, Palmer AK, Levinsohn EM. The role of radiography and computerized tomography in the diagnosis of subluxation and dislocation of the distal radioulnar joint. J Hand Surg Am 1983;8(01):23–31
24 Wechsler RJ, Wehbe MA, Rifkin MD, Edeiken J, Branch HM. Computed tomography diagnosis of distal radioulnar subluxation. Skeletal Radiol 1987;16(01):1–5
25 Chiang CC, Chang MC, Lin CF, Liu Y, Lo WH. Computerized tomography in the diagnosis of subluxation of the distal radioulnar joint. Zhonghua Yi Xue Za Zhi (Taipei) 1998;61(12):708–715

26 Geissler WB. Carpal fractures in athletes. Clin Sports Med 2001;20 (01):167–188
27 Gelberman RH, Menon J. The vascularity of the scaphoid bone. J Hand Surg Am 1980;5(05):508–513
28 Adams JE, Steinmann SP. Acute scaphoid fractures. Hand Clin 2010;26(01):97–103
29 Cheung GC, Lever CJ, Morris AD. X-ray diagnosis of acute scaphoid fractures. J Hand Surg [Br] 2006;31(01):104–109
30 Adey L, Souer JS, Lozano-Calderon S, Palmer W, Lee SG, Ring D. Computed tomography of suspected scaphoid fractures. J Hand Surg Am 2007;32(01):61–66
31 O'Shea K, Weiland AJ. Fractures of the hamate and pisiform bones. Hand Clin 2012;28(03):287–300, viii
32 Norman A, Nelson J, Green S. Fractures of the hook of hamate: radiographic signs. Radiology 1985;154(01):49–53
33 Scalcione LR, Gimber LH, Ho AM, Johnston SS, Sheppard JE, Taljanovic MS. Spectrum of carpal dislocations and fracture-dislocations: imaging and management. AJR Am J Roentgenol 2014;203(03):541–550
34 Mayfield JK, Johnson RP, Kilcoyne RK. Carpal dislocations: pathomechanics and progressive perilunar instability. J Hand Surg Am 1980;5(03):226–241

